Reflectance Decreases before Thickness Changes in the Retinal Nerve Fiber Layer in Glaucomatous Retinas

Xiang-Run Huang,[1,2] *Ye Zhou,*[2] *Wei Kong,*[1] *and Robert W. Knighton*[1]

Purpose. Glaucoma damages the retinal never fiber layer (RNFL). RNFL thickness, measured with optical coherence tomography (OCT), is often used in clinical assessment of the damage. In this study the relation between the RNFL reflectance and thickness at early stages of glaucoma was investigated.

Methods. A rat model of glaucoma was used that involved laser photocoagulation of the trabecular meshwork. The reflectance of the RNFL in an isolated retina was measured, followed by immunohistochemical staining of the axonal cytoskeleton. RNFL thickness was measured by confocal fluorescence imaging. RNFL reflectance was calculated for bundle areas located at radii of 0.22, 0.33, and 0.44 mm from the optic nerve head (ONH) center. Linear regression was used to study the relation between reflectance and thickness. For glaucomatous eyes, only those bundles with no apparent structural damage were used.

Results. Bundles in 11 control retinas and 10 treated retinas were examined. Bundle thickness of both groups at each radius was similar ($P = 0.89$). The reflectance of the bundles at radii of 0.33 and 0.44 mm was found to be similar in both control and treated retinas ($P > 0.5$). However, the reflectance of the bundles at the 0.22-mm radius decreased significantly in the treated group ($P = 0.005$).

Conclusions. Elevation of intraocular pressure causes decrease in RNFL reflectance for bundles near the ONH. Change in RNFL reflectance precedes thinning of the RNFL. The results suggest that a decrease in RNFL reflectance near the ONH is an early sign of glaucomatous damage. (*Invest Ophthalmol Vis Sci.* 2011;52:6737–6742) DOI:10.1167/iovs.11-7665

The retinal nerve fiber layer (RNFL) consists of axons of retinal ganglion cells (RGCs). Glaucomatous damage to the RNFL usually precedes detectable visual field loss, and direct assessment of the RNFL is therefore often used in clinical diagnosis of the disease. Common optical diagnostic methods, such as optical coherence tomography (OCT), use light reflected from the RNFL to assess the change in thickness during the development of glaucoma. Knowledge of the reflectance property of the RNFL in diseased retina can enhance the interpretation of clinical measurements and improve detection of damage or progression of the disease.

RNFL reflectance in normal retinas has the following characteristics: (1) The reflectance is very directional.[1] A nerve fiber bundle is visible only when the reflected light is measured in a conical sheet concentric with the bundle axis. The directionality suggests that RNFL reflectance arises from light-scattering by the cylindrical structures of axons.[2] (2) RNFL reflectance is proportional to its thickness.[3] Proportionality implies that the reflected light arises from throughout the entire volume of a nerve fiber bundle. (3) RNFL reflectance declines with increasing wavelength. Wavelength dependence implies that different scattering mechanisms underlie RNFL reflectance at different wavelengths.[4] (4) With the use of colchicine, studies have identified microtubules as one contributor to the RNFL reflectance,[5,6] yet other scattering components are not clear.

Glaucoma damages axons of RGCs.[7–14] The degree of damage varies from distortion of axonal ultrastructure to total loss of axons. Immunohistologic studies show that elevation of intraocular pressure (IOP) causes alteration of the axonal cytoskeleton, and such cytostructural distortion precedes macroscopic change in the RNFL. Hence, cytostructural change is an early sign of RNFL damage.

Because RNFL reflectance arises from light scattering by the ultrastructure in axons,[15] changes in the axonal cytoskeleton must cause changes in RNFL reflectance. In this study, we used a rat model of glaucoma to investigate the relation between RNFL reflectance and its thickness at early stages of glaucomatous damage. The knowledge gained will be helpful in understanding early pathologic states of axonal degeneration.

Material and Methods

Rat Model of Glaucoma

Female Wistar rats weighing 250 to 350 g were used. The animals were housed in a 12-hour light–12-hour dark cycle, with standard food and water provided ad libitum. Experimental glaucoma was induced by translimbal laser photocoagulation of the trabecular meshwork.[16] Animals were anesthetized with intraperitoneal ketamine (50 mg/kg) and xylazine (5 mg/kg) and topical proparacaine 1% eye drops. The laser treatment (a diode laser with wavelength of 532 nm, 500-mW power, 0.6-second duration, and 50-μm diameter spot size) was administered to the left eye of each rat. Approximately 55 to 60 trabecular burns were evenly distributed. After a week, a second treatment was applied to those eyes that did not maintain elevated IOP. The contralateral eye was untreated and served as the control.

A rebound tonometer (Tonolab; Icare, Helsinki, Finland) was used to monitor IOP after the animals were deeply anesthetized. IOP in both eyes was measured just before treatment and 1, 3, 5, and 7 days after treatment and then once a week, until enucleation or until IOP returned to baseline.

All experiments adhered to the ARVO Statement for the Use of Animals in Ophthalmic and Vision Research. The protocol for the use of animals was approved by the Animal Care and Use Committee of the University of Miami.

From the [1]Bascom Palmer Eye Institute and the [2]Department of Biomedical Engineering, University of Miami, Miami, Florida.

Supported by National Institutes of Health Grant R01-EY019084, American Health Assistance Foundation G2008-033, National Institutes of Health Core Grant P30-EY014801, Research to Prevent Blindness, and a Department of Defense Career Development Award.

Submitted for publication April 1, 2011; revised May 12 and June 22, 2011; accepted June 24, 2011.

Disclosure: **X.-R. Huang**, None; **Y. Zhou**, None; **W. Kong**, None; **R.W. Knighton**, None

Corresponding author: Xiang-Run Huang, Bascom Palmer Eye Institute, University of Miami Miller School of Medicine, 1638 NW Tenth Avenue, Miami, FL 33136; xhuang3@med.miami.edu.

Tissue Preparation

Three weeks after the first laser treatment, both eyes of each animal were used in the study. Tissue preparation followed previously developed procedures.[17] Briefly, one eye of an anesthetized animal was removed and prepared for optical measurements. After completion of the first eye's measurement, the other eye was removed and subjected to the same experimental procedures. The animal was then euthanatized. For each eye, an eye cup of 5-mm diameter that included the optic nerve head (ONH) at the center of the eye cup was excised and placed in a dish of warm (33–35°C) oxygenated physiologic solution. The retina was dissected from the retinal pigment epithelium and choroid and then draped across a slit in a black membrane with the photoreceptor side against the membrane. A second, thinner membrane with a slit matched to the black membrane was put on the RNFL surface to gently stretch the retina and eliminate wrinkles. The above procedure was performed with intense white illumination, which thoroughly bleached the visual pigment in the photoreceptors and ensured that the reflectance in this layer remained constant. The mounted retina was placed in a chamber perfused with warm physiologic solution to keep the tissue alive.

Measurement of RNFL Reflectance

A multispectral imaging microreflectometer was used to detect the reflectance of the RNFL. The device has been described in detail previously.[4] Briefly, light from a tungsten-halogen lamp followed by an interference filter (10-nm full width at half maximum) provided monochromatic illumination to a retina. The mounted retina was placed in the chamber at the center of a spherical window. It was imaged onto a cooled, charge-coupled device (CCD) (U47+ Digital Imaging System; Apogee Instruments, Inc., Logan, UT) that provided a digital resolution of 2.2 μm/pixel in an aqueous medium and a full field of view of 2.3 $\times$ 2.3 mm on the retina. The chamber was mounted on a precision stage that could be adjusted for translation and rotation. The optical axes of light source and camera, both approximately intersecting at the center of the spherical window, could also be moved.

In the experiments, the bundles were oriented approximately vertically, and the camera and light source were adjusted to the positions that gave near maximum (on-peak) reflectance of the nerve fiber bundles, with a dark, uniform background.

Images of the RNFL were collected by the CCD camera at wavelengths ranging from 400 to 830 nm. Exposure duration of the CCD camera was selected to ensure that no saturation occurred in any images at any wavelength. Black images taken with the same exposure duration, but with the light source off, were subtracted from each image, to compensate for the dark current and bias level of the CCD. The resulting pixel values were directly proportional to the reflected intensity. The pixel values were then converted to relative diffuse reflectance using images of a diffuse white reflector (6080 White Reflectance Coating; Eastman Kodak Company, Rochester, NY). Hereafter, the relative reflectance is simply called reflectance.

Calculation of RNFL Reflectance

To calculate the reflectance of nerve fiber bundles, bundle areas were selected at distances of approximately 0.22, 0.33, and 0.44 mm (r_a, r_b, and r_c) from the ONH center, which was defined as the convergence point of nerve fiber bundles within the ONH. At each radius, one to three bundles was selected from each retina. If more than one bundle was selected, they were separated by at least one major blood vessel. The RNFL reflectance was calculated for those bundles, which were measured at on-peak reflectance and had approximately uniform gap areas between the bundles. Reflectance measured on bundle areas included light reflected from the RNFL and its underlying tissue. Because the weak scattering of the RNFL caused little attenuation of the incident beam, we assumed that the reflectance from deep layers was approximately the same as that from nearby gap areas. Rectangular areas, each containing approximately 10 pixels, were chosen from the bundles and from the nearby gaps between bundles. The average reflectance of gap areas was then subtracted from the total reflectance measured on the bundle areas to get an estimate of the bundle reflectance alone. The reflectance of several closely defined areas on the same bundle was then averaged. Because RNFL reflectance depends on wavelengths, mean reflectance at wavelengths of 400 to 420, 500 to 560, and 740 and 830 nm were calculated.

The incident and scattering angles for the measured bundle area were also calculated based on the properties of light-scattering from a cylinder, which constrains all scattered rays to lie in a conical sheet concentric with the axis of the bundle. The incident angle was defined as the angle between the incident ray and a plane perpendicular to the bundle; the scattering angle was defined as the angle between incident and scattering planes, where the incident plane contained the incident ray, and the bundle and the scattering plane contained the reflected ray and the bundle. The backscattering angle was 180°. In the experiments, the incident and scattering angles were estimated from the orientation of a bundle's projection in an image and the positions of the light source and camera in the laboratory coordinate system. A detailed description of the scattering geometry can be found in an earlier publication.[4] Only those bundles with similar incident and scattering angles were used for data comparison.

To compensate for possible tissue shift during the measurement, the entire set of images was registered by horizontal and vertical translation.

Confocal Laser Scanning Imaging

After reflectance measurement, a retina was fixed in 4% paraformaldehyde for 30 minutes at room temperature and rinsed thoroughly in phosphate-buffered saline (PBS). The tissue was then removed from the membranes for immunohistochemical staining. Three major cytoskeletal components of axons were labeled in a whole-mounted retina with phalloidin to stain F-actin, anti-β-tubulin monoclonal antibody to mark microtubules, and anti-neurofilament antibody to label neurofilaments. Nuclei in the inner retina were also identified by 4′,6-diamidino-2-phenylindole (DAPI) fluorescent counterstain. The detailed procedure for fluorescence staining is described in a recently published paper.[14]

Confocal imaging of a stained retina was performed according to a previously developed procedure.[9,14] Briefly, a confocal laser scanning microscope (TCS SP5; Leica Microsystems, Bannockburn, IL) was used to provide both en face and cross-sectional images of a whole-mounted retina. A 40× oil objective provided en face images of the tissue, with a full field view of 389 $\times$ 389 μm and a resolution limited to the sampling density of 0.76 μm/pixel. To cover bundles around the ONH, at least a 3 $\times$ 3 tiled array of images was taken that covered a retinal area of 1.2 $\times$ 1.2 mm with the ONH at the center. To measure RNFL thickness, en face images were collected in each array position at evenly spaced depths (1 μm apart in tissue), starting from the RNFL surface through the retina, to a depth at least including the ganglion cell layer. The retina was then reconstructed in 3-D, and cross-sectional images were synthesized from the reconstruction with customized software.

Measurement of RNFL Thickness

To relate measured optical properties of the RNFL to its underlying cytostructure, the location of an individual nerve fiber bundle measured optically was identified in the corresponding confocal image of the same retina with a procedure modified from a previously developed method.[18] Briefly, the en face confocal image of a retina (Fig. 1A) was registered onto the optical image of the same retina (Fig. 1B) by matching the blood vessel patterns. The bundle areas that were originally defined in the optical image were then marked in the confocal image. To determine the cross-sectional image of the bundle, a line across the area and perpendicular to the bundle was defined. The cross-sectional image along the line was obtained from a reconstructed 3-D confocal laser scanning microscopy (cLSM) image. The thickness of the selected nerve fiber bundle was measured from the

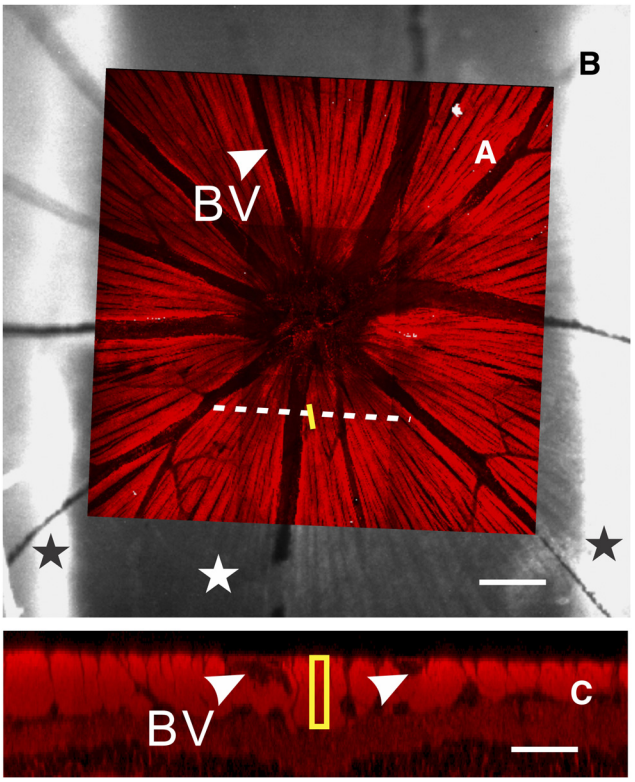

FIGURE 1. Image registration and measurement of RNFL thickness. (**A**) En face confocal image of a normal retina (40× objective). Bright stripes are retinal nerve fiber bundles with fluorescent stain of microtubules. The image is registered to the reflectance image of the retina in (**B**). *Yellow line*: a bundle area selected for reflectance analysis. *Dashed line*: defined to derive a cross-sectional image of the bundles. (**B**) Reflectance image obtained at 440 nm. *Black stars*: portions of retina held by the mounting membranes; *white star*: retinal area across the slits of the membranes. Bundle reflectance was measured in this region. (**C**) Cross-sectional image along the *dashed line* in (**A**). Bundle thickness was measured as the length of the rectangle. *Arrowheads* and BV: blood vessels. Scale bar: (**B**) 100 μm; (**C**) 50 μm horizontally; 25 μm vertically.

image as the length of a rectangle that passed through the center of the bundle (Fig. 1C).

Data Analysis

The purpose of this study was to investigate the change in RNFL reflectance at early stages of glaucomatous damage. Because RNFL reflectance depends on the geometric settings of a measurement, data were selected by using the following procedure: (1) Bundles measured at on-peak reflectance were chosen, and the incident and scattering angles were calculated; (2) the bundles with incident angles between 10° and 30° and scattering angles between 160° and 180° were selected; (3) confocal images of these bundles were examined. Bundles were excluded if any cytoskeletal components appeared distorted in the confocal images.

In normal retinas, RNFL reflectance is proportional to its thickness. In this study, linear regression was used to fit a scatterplot of bundle reflectance and thickness. The regression used a straight line $y = \boldsymbol{m}x + b$, where y is reflectance, x is thickness in micrometers, the slope $\boldsymbol{m}$ is the proportionality constant between reflectance and thickness in units of reflectance per micrometer, and b is the y intercept representing a constant reflectance added to all points.

Reconstruction of 3-D confocal image and measurements of RNFL reflectance and thickness were implemented with customized software (programmed in MatLab; The MathWorks, Inc. Natick, MA). Image registration was implemented in image-management software (CorelDraw Version 11; Corel Corporation, Ottawa, ON, Canada).

Bundle thickness was compared with a linear mixed-model analysis accounting for the correlation between multiple measurements made on the same retina and post hoc least-significant-difference tests. Incident angle and scattering angles were compared in an unequal variance *t*-test. The influence of treatment group and bundle location on the proportionality constant was studied with the analysis of covariance formulation of the general linear model, which included tests of proportionality constant and group interactions (SPSS/PASW Statistics 18; IBM Corporation, Somers NY). The significance level was set at $P < 0.05$.

RESULTS

Fourteen Wistar rats were treated unilaterally. The mean IOP increased from 11 ± 0.5 to 41 ± 8 mm Hg. The IOP of all treated eyes remained elevated for about 2 weeks. Bundles that satisfied the selection criteria described above were measured in 11 control and 10 treated retinas. Bundle thickness (mean ± SD) at each radius was compared between the control and treated retinas (Table 1). There was no difference between the control and treated retinas ($P = 0.89$). However, in both groups r_a was significantly thicker than both r_b and r_c ($P < 0.001$), but r_b and r_c were not different from each other ($P = 0.10$). The incident and scattering angles were not different between the groups ($P > 0.6$), with the average incident angles of 18° ± 6° and 19° ± 6° for control and treated retinas, respectively, and average scattering angles of 170° ± 6° for both groups.

Axonal Cytoskeleton in Retinas with Elevated IOP

All treated retinas showed different degrees of structural damage. Figure 2 demonstrates a treated retina with localized alteration of cytoskeleton. Around the ONH, the area with normal-looking bundles (Fig. 2A, solid box) had approximately uniform stain of F-actin, microtubules, and neurofilaments within the bundles (Fig. 2B). However, localized damage occurred in the same retina. Figure 2C showed distorted structure in all cytoskeletal components. Wavy strands of cytoskeletal components ran along the bundles. Aberrant strands of F-actin and neurofilaments crossed the bundles. Nuclei were abundant and embedded within the bundles. Detailed studies of the cytoskeletal change have been published separately.[9] In this study, the confocal images were used to identify normal-looking bundles and calculate their thickness as described in Figure 1C.

RNFL Reflectance and Spectrum

In normal retinas, nerve fiber bundles stand out in high-contrast against a darker background. The bundles measured near on-peak reflectance appeared as bright stripes (Fig. 3A). However, the reflectance further along the same bundles decreased due to a tilt of the retinal tissue. In this study only bundle

TABLE 1. Average Bundle Thickness at Different Distances (*r*) from the ONH

	Thickness (μm)		
	r_a = 0.22 mm	r_b = 0.33 mm	r_c = 0.44 mm
Control	21 ± 10 (22)	14 ± 4 (20)	12 ± 5 (13)
Treated	22 ± 10 (21)	16 ± 5 (21)	14 ± 4 (17)

Data in parentheses are the total number of bundles analyzed.

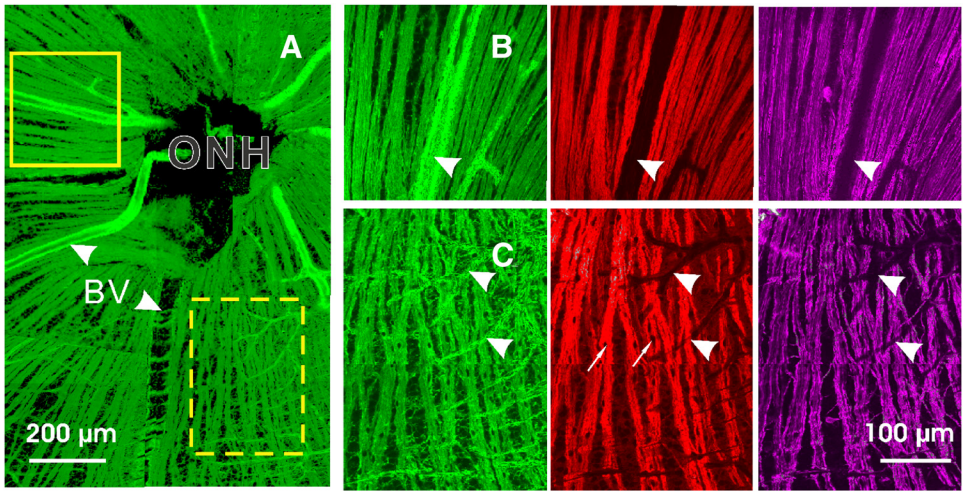

FIGURE 2. RNFL assessment by confocal microscopy (40× objective). The treated retina had simultaneous fluorescent staining with F-actin (*green*), microtubules (*red*), and neurofilaments (*magenta*). (**A**) A montage of the en face images of the RNFL with F-actin stain. (**B**) Enlarged view of the *solid box* in (**A**) with 90° rotation. Normal-looking bundles appear as bright stripes with uniform staining of cytoskeletal components within and along the bundles. (**C**) Enlarged view of the *dashed box* in (**A**). Altered cytostructure shows distorted strands of cytoskeletal components. Nuclei (*arrows*), identified by DAPI stain (not shown) are embedded in the bundles. *Arrowheads* and BV: blood vessels.

regions measured at on-peak reflectance were selected for data analysis.

RNFL reflectance is wavelength dependent. Figure 3B shows a reflectance spectrum of the bundle area marked in Figure 3A. The reflectance was higher at short wavelengths and declined with increasing wavelength.

In retinas with mild glaucomatous damage, bundles still appeared as bright stripes against a dark background, but had lower contrast compared with normal bundles. Figure 3B compares the reflectance spectra of one bundle each in control and treated retinas. Both bundles had a thickness of 26 μm and were measured at a similar geometric setting (19° and 172° incident and scattering angles, respectively). The pattern of reflectance spectra was similar. However, the bundle reflectance in the treated retina was lower at all wavelengths.

Relation between RNFL Reflectance and Thickness

The relation between RNFL reflectance and thickness was studied at different distances away from the ONH center. Figure 4A demonstrates the relation in bundle areas selected at a distance of 0.33 mm from the center of the ONH. The scatterplot shows that for both control and treated retinas the bundle reflectance was approximately proportional to its thickness. A linear fitting of the data gave a proportionality constant $\boldsymbol{m}$, which represented an average reflectance per micrometer thickness of the RNFL. At the distances of 0.33 and 0.44 mm (data not shown), the fitted $\boldsymbol{m}$ (± SE) was equal to 0.07% ± 0.01%/μm for both the control and treated groups. For bundle areas near the ONH (Fig. 4B, r_a = 0.22 mm), the bundle reflectance of both groups also increased with increasing thickness. However, linear regression fitting showed that the slope of the treated group was significantly lower than that of the control (P = 0.005).

Figure 5 summarizes fitted $\boldsymbol{m}$ at different radii for each wavelength. For the control retinas at any wavelength $\boldsymbol{m}$ was similar along bundles ($P > 0.7$). For bundle areas near the ONH $\boldsymbol{m}$ of the treated retinas was significantly lower than that of the control at each corresponding wavelength (P = 0.003, 0.005, and 0.02 for $\boldsymbol{m}$ measured at 400–440, 500–560, and 740–830 nm, respectively). In contrast, in the peripheral regions $\boldsymbol{m}$ of the treated retinas was similar to that of the control at all wavelengths ($P > 0.5$).

DISCUSSION

In clinical assessment of RNFL with optical methods such as OCT and scanning laser ophthalmoscopy, RNFL reflectance is often used to derive the thickness of RNFL. The RNFL thickness then is used for diagnosis and management of glaucoma and other optic neuropathologic diseases. However, preliminary OCT evidence from glaucomatous patients shows that change in RNFL reflectance precedes loss of RNFL thickness.[19] In this study, we used a rat model of glaucoma and in vitro retinal preparations with carefully controlled reflectance geometry to study the relation between the RNFL reflectance and thickness at early stages of glaucomatous damage.

Optically, the RNFL is a highly reflective layer in the retina. The RNFL reflectance is very directional, so that the reflectance of the RNFL depends on the geometric settings of reflectance

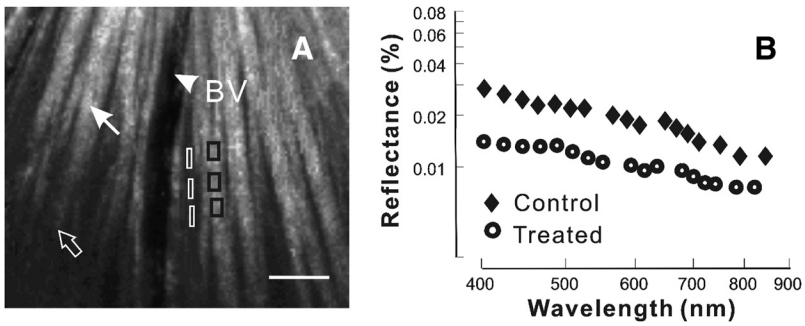

FIGURE 3. Reflectance of retinal nerve fiber bundles. (**A**) Reflectance image (440 nm) of a normal retina. At near on-peak, reflectance bundles (*white arrow*) appear as bright stripes against a darker background. The same bundles (*open arrow*) become dim at off-peak reflectance due to tissue tilt. *Black boxes*: bundle areas selected for reflectance analysis; *white boxes*: gap areas selected for background subtraction of the nearby bundle areas. *Arrowhead* and BV: blood vessel. Scale bar: 50 μm. (**B**) Reflectance spectra plotted on log-log coordinates. Reflectance was derived from bundle areas near the ONH (r_a = 0.22 mm) in control and treated retinas. Bundle reflectance of both retinas decreased with increasing wavelength. However, the reflectance of the treated retina was lower than the control at all wavelengths.

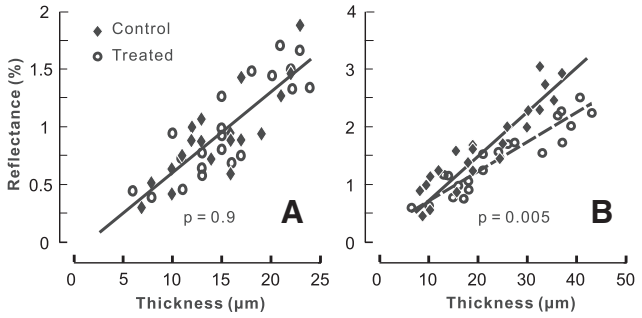

FIGURE 4. Relation between average RNFL reflectance at 500 to 560 nm and thickness. The RNFL reflectance increased with increasing thickness. Bundle areas selected at $r_b = 0.33$ mm (**A**) and $r_a = 0.22$ mm (**B**). Linear regression parameters (± SE): (**A**) $\boldsymbol{m} = 0.07\% \pm 0.01\%/\mu m$ and $b = -0.11\% \pm 0.17\%$ with $R^2 = 0.69$ for the control group; $\boldsymbol{m} = 0.07\% \pm 0.01\%/\mu m$ and $b = -0.12\% \pm 0.16\%$ with $R^2 = 0.73$ for the treated group. The two fitted lines overlap. (**B**) $\boldsymbol{m} = 0.07\% \pm 0.01\%/\mu m$ and $b = 0.04\% \pm 0.17\%$ with $R^2 = 0.85$ for the control group; $\boldsymbol{m} = 0.05\% \pm 0.01\%/\mu m$ and $b = 0.21\% \pm 0.13\%$ with $R^2 = 0.84$ for the treated group.

measurements. We showed that RNFL reflectance measured at on-peak reflectance was proportional to thickness in normal retinas. The proportional relation between reflectance and thickness suggests that the reflected light arises from the entire volume of a nerve fiber bundle. A corollary of the proportional relation is that the cytostructure contributing to the RNFL reflectance distributes approximately uniformly within a nerve fiber bundle. In normal rodent retinas, microtubules contribute approximately 50% to the RNFL reflectance,[6] and electron microscopy and immunohistological staining demonstrate approximately uniform distribution of microtubules in the RNFL.[20] Other cytostructures contributing to the RNFL reflectance are not identified yet. Understanding characteristics of scattering structure distribution within the RNFL aids interpretation of signals measured by techniques using reflected light. For example, reflectance signals with depth resolution, such as A-scans obtained by OCT, should be approximately constant when a light beam scans through a retinal nerve fiber bundle; that is, the magnitude of the signal should not change very much along the scan path within the bundle.

The proportionality constant $\boldsymbol{m}$ represents reflectance per thickness of RNFL. In normal retinas, $\boldsymbol{m}$ did not change significantly along bundles, suggesting that the composition and distribution of scattering structures are similar along bundles. Because of the dependence of RNFL reflectance on wavelength (Fig. 3B), $\boldsymbol{m}$ also varied with wavelength in normal retinas.

In this study, retinas exposed to elevated IOP were used to determine the change in RNFL reflectance occurring in early stages of glaucoma. We found a decrease in bundle reflectance of bundles near the ONH. However, the reflectance of the bundles farther from the ONH did not show significant change compared with the control. This result indicates that nerve fiber bundles near the ONH are more vulnerable to damage caused by elevated IOP. The finding is consistent with the early immunohistological studies of retinas in a rat model of glaucoma, in which F-actin in the portion of a bundle near the ONH is found to be altered while the peripheral regions in the same bundle still appear intact and RGC loss occurs first near the ONH.[21] In a recent study of the pattern of RNFL defects in glaucomatous patients, a significant proportion of mildly glaucomatous eyes are found to have RNFL defects near the ONH while the parapapillary RNFL thickness is normal as measured by OCT.[22] These results support that the site of primary damage in glaucoma is at the ONH, one of the most often suspected sites damaged by IOP elevation. The goal of this study was to investigate reflectance change at early stages of glaucomatous damage. Confocal images of immunofluorescence-stained cytoskeletal components, including F-actin, microtubules, and neurofilaments, were used to assess structural change in the retinas. The bundles used in this study were specifically selected—that is, the selected bundles did not have apparent distortion in any of these cytoskeletal components (Fig. 2A) and, in addition, the bundle thickness in the treated and control groups was similar (Table 1). Hence, the result, a decrease in RNFL reflectance, suggests that a change in RNFL reflectance occurred before the apparent change in axonal cytoskeleton and detectable thinning of the RNFL. Decrease in reflectance of bundles near the ONH can perhaps identify an early state of axonal degeneration in which irreversible damage to the axons of ganglion cells can be prevented.

Glaucoma damages axonal ultrastructure.[8,10–13] At early stages of damage, structural change precedes thinning of the RNFL. This evidence is consistent with the current finding that RNFL reflectance decreases before thinning of the RNFL. Moreover, in this study, we found that a decrease in RNFL reflectance occurred before an alteration of the cytoskeleton was observed. This result conflicts with our expectation that a change in bundle reflectance should relate to change in axonal cytoskeleton. RNFL birefringence, an optical property of RNFL due to preferentially oriented cytostructure, is also found to change before a detectable loss of RNFL thickness.[23] Because both reflectance and birefringence of RNFL are determined by the distribution and relative refractive index of the RNFL ultrastructure, one possibility is that early glaucomatous damage changes the optical properties of extracellular and/or cytoplasmic constituents before distorting the cytoskeleton.[24] Because in this study the cytostructural distribution was evaluated without quantifying structural density, an alternative explanation could be that a decrease in cytoskeletal density occurs before structural distortion to produce the decrease in RNFL reflectance. Alternatively, another cytostructure not stained in this study, such as the axonal membrane, may contribute to the RNFL reflectance. In future studies, a more refined analysis, such as electron microscopy, might be necessary to identify the anatomic and pathologic basis for change of the RNFL reflectance.

In summary, RNFL reflectance decreases before thinning of the RNFL. Measuring reflectance change in bundles near the ONH is a sensitive way to detect early glaucomatous damage, which may open a therapeutic window during which damage of axonal structure may be prevented.

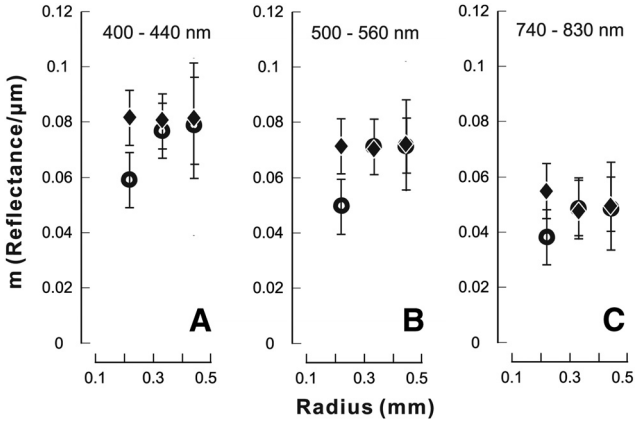

FIGURE 5. Proportionality constant $\boldsymbol{m}$ at different retinal locations and wavelengths. For the bundles near the ONH $\boldsymbol{m}$ decreased significantly in the treated retinas at all wavelengths. Vertical bars: ±SE of the fitting.

Acknowledgments

The authors thank William J. Feuer, Joyce Schiffman, and Wei Shi for statistical consultations and analyses.

References

1. Knighton RW, Baverez C, Bhattacharya A. The directional reflectance of the retinal nerve fiber layer of the toad. *Invest Ophthalmol Vis Sci.* 1992;33:2603–2611.
2. Zhou Q, Knighton RW. Light scattering and form birefringence of parallel cylindrical arrays that represent cellular organelles of the retinal nerve fiber layer. *Appl Opt.* 1997;36:2273–2285.
3. Knighton RW, Zhou Q. The relation between reflectance and thickness of the retinal nerve fiber layer. *J Glaucoma.* 1995;4:117–123.
4. Knighton RW, Huang X-R. Directional and spectral reflectance of the rat retinal nerve fiber layer. *Invest Ophthalmol Vis Sci.* 1999; 40:639–647.
5. Knighton RW, Huang X-R, Zhou Q. Microtubule contribution to the reflectance of the retinal nerve fiber layer. *Invest Ophthalmol Vis Sci.* 1998;39:189–193.
6. Huang X-R, Knighton RW, Cavuoto LN. Microtubule contribution to the reflectance of the retinal nerve fiber layer. *Invest Ophthalmol Vis Sci.* 2006;47:5363–5367.
7. Soto I, Oglesby E, Buckingham BP, et al. Retinal ganglion cells downregulate gene expression and lose their axons within the optic nerve head in a mouse glaucoma model. *J. Neurosci.* 2008; 28:548–561.
8. Fu CT, Sretavan D. Laser-induced ocular hypertension in albino CD-1 mice. *Invest Ophthalmol Vis Sci.* 2010;51:980–990.
9. Huang X-R, Knighton RW. Altered F-actin distribution in retinal nerve fiber layer of a rat model of glaucoma. *Exp Eye Res.* 2009; 88:1107–1114.
10. Balaratnasingam C, Morgan WH, Bass L, Cringle SJ, Yu D-Y. Time-dependent effects of elevated intraocular pressure on optic nerve head axonal transport and cytoskeleton proteins. *Invest Ophthalmol Vis Sci.* 2008;49:986–999.
11. Schlamp CL, Li Y, Dietz JA, Janssen KT, Nickells RW. Progressive ganglion cell loss and optic nerve degeneration in DBA/2J mice is variable and asymmetric. *Neuroscience.* 2006;7:66.
12. Buckingham BP, Inman DM, Lambert W, et al. Progressive ganglion cell degeneration precedes neuronal loss in a mouse model of glaucoma. *J. Neurosci.* 2008;28:2735–2744.
13. Howell GR, Libby RT, Jakobs TC, et al. Axons of retinal ganglion cells are insulted in the optic nerve early in DBA/2J glaucoma. *J Cell Biol.* 2007;179:1523–1537.
14. Huang X, Kong W, Zhou Y, Gregori G. Distortion of axonal cytoskeleton: an early sign of glaucomatous damage. *Invest Ophthalmol Vis Sci.* 2011;52:2879–2888.
15. Huang X-R, Knighton RW. Microtubules contribute to the birefringence of the retinal nerve fiber layer. *Invest Ophthalmol Vis Sci.* 2005;46:4588–4593.
16. Levkovitch-Verbin H, Quigley HA, Martin KRG, Valenta D, Baumrind LA, Pease ME. Translimbal laser photocoagulation to the trabecular meshwork as a model of glaucoma in rats. *Invest Ophthalmol Vis Sci.* 2002;43:402–410.
17. Knighton RW, Huang X-R. Visible and near-infrared imaging of the nerve fiber layer of the isolated rat retina. *J Glaucoma.* 1999;8: 31–37.
18. Huang X-R, Knighton RW, Shestopalov V. Quantifying retinal nerve fiber layer thickness in whole-mounted retina. *Exp Eye Res.* 2006; 83:1096–1101.
19. Huang D, Kirschbaum A. *Glaucoma Diagnosis Based on Nerve Fiber Layer Signal Ratio in Optical Coherence Tomography.* Second Annual Meeting on Optical Coherence Tomography. Long Boat Key, Florida, 2000.
20. Pocock GM, Aranibar RG, Kemp NJ, Specht CS, Markey MK, Rylander HG. The relationship between retinal ganglion cell axon constituents and retinal nerve fiber layer birefringence in the primate. *Invest Ophthalmol Vis Sci.* 2009:50:5238–5246.
21. Yu S, Tanabe T, Yoshimura N. A rat model of glaucoma induced by episcleral vein ligation. *Exp Eye Res.* 2006;83:758–770.
22. Leung CKS, Choi N, Weinreb RN, et al. Retinal nerve fiber layer imaging with spectral-domain optical coherence tomography: pattern of RNFL defects in glaucoma. *Ophthalmology.* 2010;117: 2337–2344.
23. Fortune B, Cull GA, Burgoyne CF. Relative course of retinal nerve fiber layer (RNFL) birefringence, RNFL thickness and retinal function changes after optic nerve transection. *Invest Ophthalmol Vis Sci.* 2008;49:4444–4452.
24. Guo L, Moss SE, Alexander RA, Ali RR, Fitzke FW, Cordeiro MF. Retinal ganglion cell apoptosis in glaucoma is related to intraocular pressure and IOP-induced effects on extracellular matrix. *Invest Ophthalmol Vis Sci.* 2005;46:175–182.